Combined thermal and color 3D model for wound evaluation from handheld devices

Evelyn Gutierrez[a], Benjamín Castañeda[a], Sylvie Treuillet[b], and Yves Lucas[b]

[a]Pontificia Universidad Católica del Perú, Av. Universitaria 1801, San Miguel, Lima, Perú
[b]Laboratoire PRISME Polytech, 12 rue de Blois, BP 6744, 45067 Orleans cedex 2, France

ABSTRACT

Color, shape (size and volume), and temperature are important clinical features for chronic wound monitoring that could impact diagnosis and treatment. Noninvasive 3D measurement are better and more accurate than those in 2D, but expensive equipment and complexity of the setup prevent their use at hospitals. Therefore, the use of affordable and lightweight devices with straightforward protocol to acquire images for evaluations is fundamental to provide a functional and useful evaluation of the wound. In this work, an automated methodology to generate color and thermal 3D models is presented by using portable devices: a commercial mobile device with a connected portable thermal camera. The 3D model of the wound surface is estimated from a series of color images using structure-from-motion (SfM) while thermal information is overlaid to the ulcer's relief for multimodal wound evaluation. The proposed methodology contributes with a proof of concept for multimodal wound monitoring in the hospital environment with a simple hand-held shooting protocol. The system was used efficiently with 5 patients on wounds of various sizes and types.

Keywords: 3D model, thermography, chronic wounds

1. INTRODUCTION

Size, volume of the wounds are important bio-markers for evaluating wounds. Traditional evaluation involves manual measurements which are prone to human errors and might be painful for patients. In recent years, non invasive 3D imaging have increased popularity for providing color 3D models and metrics about wounds (e.g., length, width, area, and depth). They have proven to be reliable and comparable to those obtained with manual methods.[1,2] Visual 3D representation not only serves for the evaluation of the wound but is also useful to promote teleconsultation in remote areas and to motivate patients to follow a treatment and avoid complications.

However, color 3D models, are not enough as a standalone tool for wound assessment.[3] In particular, thermal information provides useful and interesting information that are not visible. Thermography has been used before to differentiate different types of wounds based on blood supply inside and outside the wound; to identify problems in the normal wound healing, or to identify serious problems such as infections.[4–11] However, only a few recent studies incorporate thermographic information to the 3D model for wound assessment.

Barone et al.[12] highlighted the combination of color and thermal imaging to propose a segmentation of the skin based on the thermal data. Their results show that segmentation using 3D thermal models can help reduce variability in the segmentation made only with colour 3D models. The study uses expensive and heavy equipment which would make its widespread implementation difficult. A more recent study[13] proposes a portable handheld device composed of stereo cameras and a thermal camera connected to a laptop computer. In this case, a special gadget to fix the three cameras is required to process the thermal 3D models. The advantage of this proposal is its low cost and the possibility of making 3D models in real time, which can be very useful in hospitals. Another recent study[10] shows a prototype system that incorporates different sources of information for wound monitoring. This study stands out for showing the potential of thermal, hyperspectral cameras and chemical detection sensors for wound monitoring. However, it requires expensive equipment and complex settings.

Further author information: (Send correspondence to Evelyn Gutierrez)
Evelyn Gutierrez: E-mail: egutierreza@pucp.edu.pe

In this study, we present a methodology for creating thermal and color 3D models using commercially available devices and using open source software to make it low cost, accessible and easy to implement in hospitals. Additionally, in this work, we propose to add the segmentation of the wound contour and segmentation of the external skin in order to calculate thermal indicators that are potentially useful for evaluation of the chronic wounds.

2. METHODOLOGY

2.1 Image Acquisition

Images were acquired using a low-cost commercial thermal camera FlirOne Pro (FLIR Systems, Inc., Oregon, USA) and mobile devices at two different hospitals: Hipólito Unanue Hospital in Lima (Peru) and Regional Hospital in Orleans (France). The FlirOne Pro thermal camera is able to capture a couple of images in one shot: a 1080x1440 pixels RGB image and a 480x640 pixels thermal image. Additionally, according to specifications, the thermal accuracy is +/-3°C or +/-5%. On the other hand, mobile devices provide high resolution RGB images: 4000x3000 pixels with the Xiaomi RedMi Pro7 used in France and 3024x4032 with the Samsung Galaxy Tab S4 used in Peru.

Prior to acquisition, patients were informed to obtain consent to participate. Then, they are asked to remain in a comfortable position and a color pattern is placed on the side to serve as a reference for adjusting the size of the 3D model. Acquisition begins with high-resolution photos that are acquired with the mobile device by making a slow circular motion to observe several points of view around the wound. Some images are then acquired with the thermal camera from different perspectives of the wound. From the process, around 40 high-resolution RGB images and 8 pairs of mixed low resolution images are acquired. Fig. 1 shows an example of the acquisition performed with the Samsung Galaxy Tab S4 and the thermal camera attached and Fig. 2 shows the camera positions.

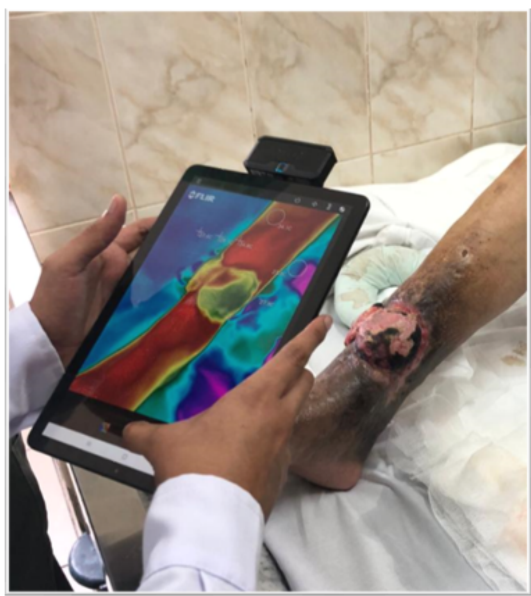

Figure 1. Portable devices are used in hand-held shooting mode for image acquisition.

2.2 Camera Calibration

The FlirOne Pro camera was calibrated once using a special planar chessboard pattern that can be detected by both the visible and the thermal camera. The materials used were a rectangular white tile and black squares made of thin black foam 1mm thick. For calibration, the pattern is cooled in the freezer for 15 minutes and

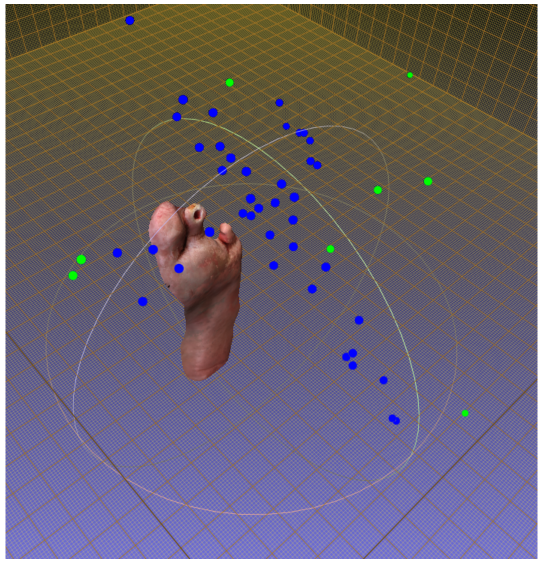

Figure 2. Several camera poses are used for creating the color and thermal 3D model. Blue points represent the RGB smartphone camera poses and green points the FlirOne Pro camera poses.

then taken outside. The black foam quickly increases its temperature while the tile remains cold resulting in a chessboard visible for both modalities.

The detection of the square corners in the chessboard images is done by a popular multiplane calibration algorithm[14] based on Harris corner detector and with an optimized alignment based on RANSAC. Fig. 3 shows the detected corners in both modalities.

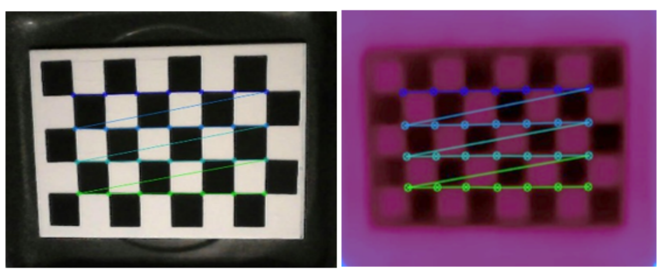

Figure 3. Color (left) and thermal image (right) of the chessboard used for FlirOne Pro camera calibration.

The calibration of each camera is done with OpenCV using 100 pairs of color and thermal images from FlirOne Pro. The re-projection error obtained was 0.0319 and 0.024 pixels for the RGB and infrared(IR) camera respectively.

2.3 Color 3D model

The 3D color model is carried out in two stages. First, using the high resolution RGB images obtained from the mobile devices and then, the low resolution RGB images from FlirOne Pro are incorporated. For each stage, the Structure from Motion algorithm (SfM) is used to estimate the 3D point cloud from keypoints obtained with SIFT algorithm. The process is completely automated using open source software: Alicevision[15] and Python.

2.4 Thermal 3D model

To add the thermal information onto the 3D model, we use the relationship between the pair of (RGB-thermal) images from the FlirOne Pro camera. The temperature is then assigned by reprojection of the 3D model on the image plane by using the estimated camera pose by the SFM algorithm.

The registration is based on an affine transformation warping the thermal image to fit onto the RGB image. Given the proximity of the RGB and IR cameras, the transformation consists only on scaling and 2D translation according to the distance between the camera and the object of interest. To model this transformation, experiments were made with the thermal chessboard pattern at different distances. Fig 4 shows an example of the registration performed between an infrared image and the corresponding RGB image.

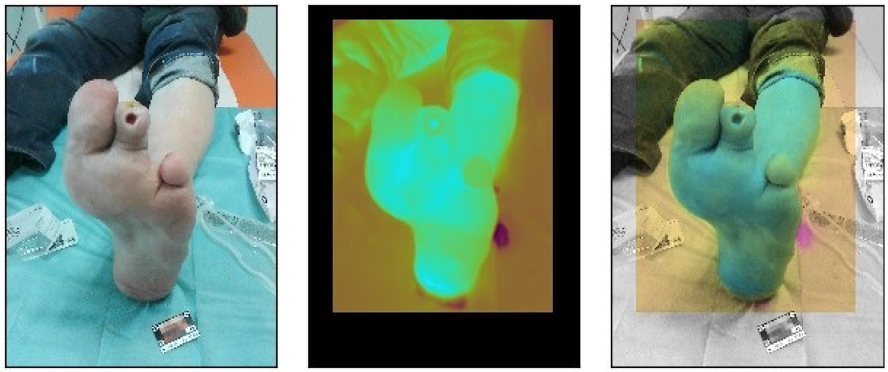

Figure 4. Low-resolution RGB image from FlirOne Pro(left); corresponding thermal image registered (center); and the overlapping of both (right).

Finally, the 3D point cloud is projected to the registered thermal image and the temperatures are assigned to each point discarding points located more than 40 cm distance to the camera and with more than 60° angle of vision to reduce errors in temperature measurement.[16]

2.5 Wound evaluation metrics

The segmentation is manually performed on the best view of the wound; and the segmented outline is then automatically re-projected to the 3D model. Note that the manual segmentation of the wound has been used for the purpose of the current proof of concept; however, automatic wound segmentation based on machine learning algorithms[17,18] could be easily incorporated into the process.

Different areas are defined related to useful indicators for the evaluation of a wound: the wound edge, the periwound, and the healthy skin around it. These areas are automatically detected from the wound outline and using the geodesic distance to take into account the curvature of the body. The wound edge is defined as a segment of 0.5 cm beyond the wound outline; the periwound extends up to 4 cm from the wound edge; and the healthy skin is defined as a segment of 2 cm distance from the periwound borders. An example of the defined areas is shown in Fig 5.

The indicators for both modalities are calculated taking into account previous studies and chronic wound care manuals.[4–11] In these studies, the potential of temperature differences between different segments of skin outside the wound and the wound-bed is shown to evidence favorable wound evolution or potential problems. Therefore, it is proposed as metrics, in addition to the area of the wound bed, the difference in temperature between the periwound and the wound (T_{PW-WB}); temperature difference between the periwound and the wound contour (T_{PW-WE}); and temperature difference between the normal reference skin and the periwound (T_{NS-PW}).

3. RESULTS

The proposed methodology was used in real patients with wounds of different sizes and located in different parts of the body. As a proof of concept, we present here five patient cases.

Fig. 6 presents the first case of an arm wound with healing problems. A low temperature is observed at the wound bed and wound edge. These are about 2°C lower compared to the peripheral area.

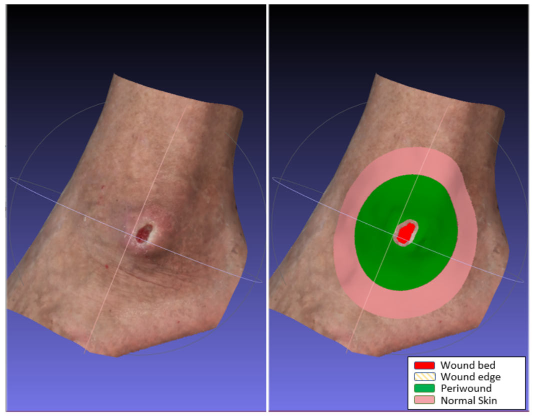

Figure 5. 3D model (right) and its corresponding areas automatically detected from the wound outline (left).

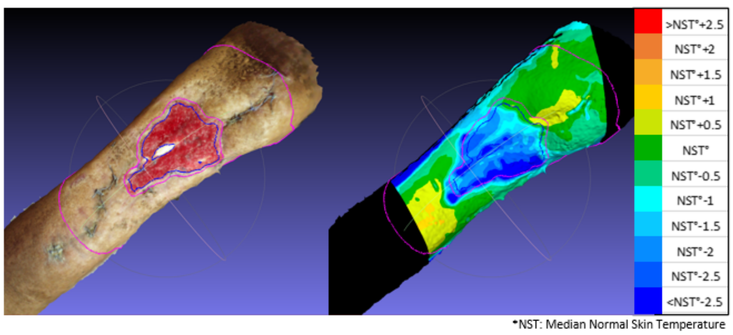

STATS		
	Median T°	**SD T°**
Wound Bed	28.11	0.84
Wound Edge	28.56	0.96
PeriWound	30.46	1.12
NormalSkin	30.26	1.99
	Diff T°	
$T_{\{PW-WB\}}$	2.35	
$T_{\{PW-WE\}}$	1.90	
$T_{\{NS-PW\}}$	-0.20	

Figure 6. Visualization of the 3D models of a wound in the arm.

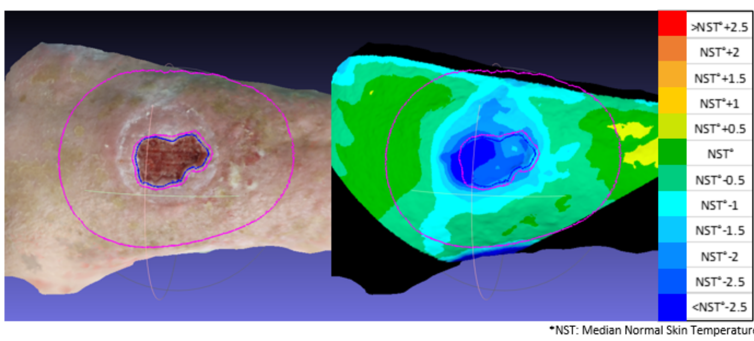

STATS		
	Median T°	**SD T°**
Wound Bed	31.22	0.35
Wound Edge	31.59	0.45
PeriWound	33.17	0.62
NormalSkin	33.45	0.47
	Diff T°	
$T_{\{PW-WB\}}$	1.95	
$T_{\{PW-WE\}}$	1.58	
$T_{\{NS-PW\}}$	0.29	

Figure 7. Color and thermal 3D models for a small wound on the foot.

In Fig. 7, a small wound is shown on one side of the foot. This wound shows a very similar pattern to the first case: the inside of the wound and contour are colder than the peripheral area with a temperature difference of about 2°C.

The following case is an ankle wound shown in Fig. 8. In this case, the temperature on the outside is higher than the median temperature in the wound bed. In addition, a lower temperature is observed at the edge of the wound. According to previous studies, this pattern corresponds to a stagnation in wound improvement. The lack of improvement in this wound was also noted by the nurses who attended this patient.

The fourth case in Fig. 9 is a toe wound that has shown some signs of healing according to the medical notes. In this case, different thermal characteristics are observed than in the previous cases. The wound is warmer than the peripheral area by about 0.8°C.

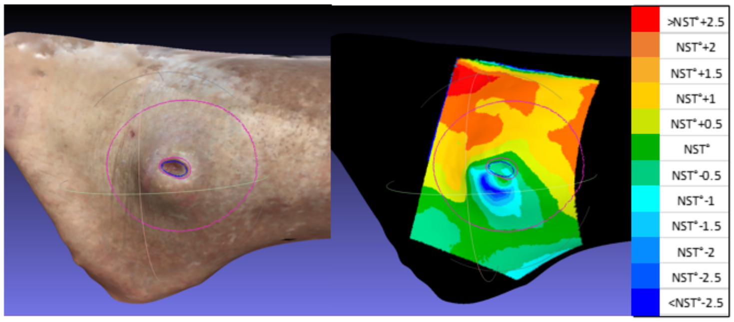

STATS		
	Median T°	SD T°
Wound Bed	28.01	0.67
Wound Edge	27.84	0.54
PeriWound	29.08	0.71
NormalSkin	28.56	0.93
	Diff T°	
$T_{\{PW-WB\}}$	1.06	
$T_{\{PW-WE\}}$	1.23	
$T_{\{NS-PW\}}$	-0.52	

*NST: Median Normal Skin Temperature

Figure 8. Color and thermal 3D models for a small ankle wound.

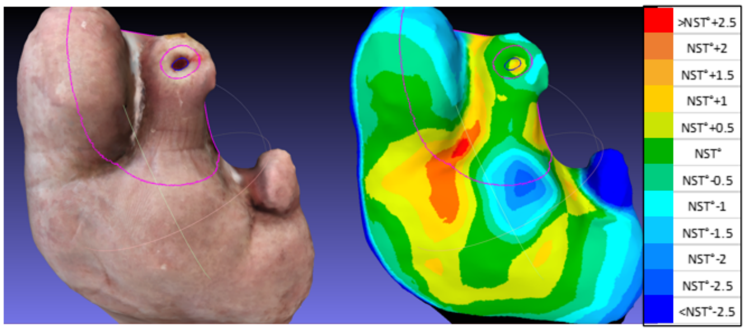

STATS		
	Median T°	SD T°
Wound Bed	32.36	0.40
Wound Edge	31.83	0.31
PeriWound	31.54	0.84
NormalSkin	31.88	1.27
	Diff T°	
$T_{\{PW-WB\}}$	-0.82	
$T_{\{PW-WE\}}$	-0.29	
$T_{\{NS-PW\}}$	0.34	

*NST: Median Normal Skin Temperature

Figure 9. Color and thermal 3D models for a small toe lesion.

As could be seen in the different cases, the temperature characteristics between the different wound segments and peripheral parts vary from case to case. In Fig 10, we can observe how these patterns change from case to case.

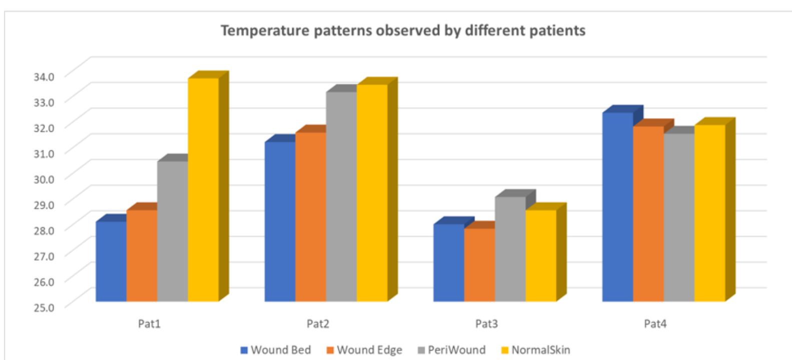

Figure 10. Comparison of the median temperatures in the different skin areas by patient.

Finally, in Fig. 11, a 3D model for a large wound between the thigh and the back is shown. It can be noted that since the system uses a camera in handheld mode, it is possible to obtain models of large areas and on curved surfaces.

4. CONCLUSION

In this study, a methodology for creating a combined color and thermal 3D model from accessible and portable devices is proposed. No complex settings or expensive equipment is required so that it could be easily integrated

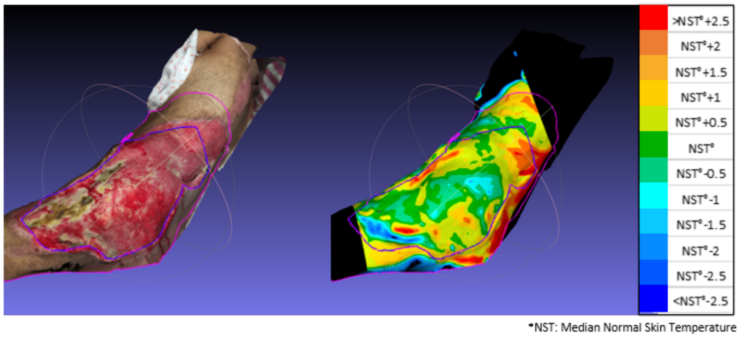

STATS	Median T°	SD T°
Wound Bed	27.71	0.75
Wound Edge	27.69	0.53
PeriWound	27.96	0.87
NormalSkin	-	-
	Diff T°	
$T_{\{PW-WB\}}$	0.25	
$T_{\{PW-WE\}}$	0.27	
$T_{\{NS-PW\}}$	-	

Figure 11. Color and thermal 3D model visualization of a large wound between the thigh and the back.

for wound evaluation. Moreover, wound segmentation in 3D models and metrics are proposed to help with evaluation and monitoring of wounds.

The main advantage of the proposed methodology is that it allows obtaining 3D thermal models of wounds located on any part of the body. In addition, the use of commercially available and affordable imaging devices could allow for remote wound assessment and monitoring. These features are an advantage over most previous approaches where the scanning area was small or required additional expensive equipment.

Future work includes refining the acquisition protocol and thermal image processing for large wounds and wounds located at the edges. In addition, we plan to incorporate automatic wound segmentation and tissue classification based on deep learning. Finally, we also intend to conduct a longitudinal study to identify metrics that can help predict, at an early stage, potential problems in the evolution of chronic wounds.

ACKNOWLEDGMENTS

This project has received funding from the European Union's Horizon 2020 research and innovation program under the Marie Sklodowska-Curie grant agreement N°777661 (STANDUP project).

REFERENCES

[1] Darwin, E. S., Jaller, J. A., Hirt, P. A., and Kirsner, R. S., "Comparison of 3-dimensional Wound Measurement With Laser-assisted and Hand Measurements: A Retrospective Chart Review," *Wound Management & Prevention* **65**, 36–41 (Jan. 2019).

[2] Bowling, F. L., King, L., Fadavi, H., Paterson, J. A., Preece, K., Daniel, R. W., Matthews, D. J., and Boulton, A. J. M., "An assessment of the accuracy and usability of a novel optical wound measurement system," *Diabetic Medicine* **26**, 93–96 (Jan. 2009).

[3] van Netten, J. J., Clark, D., Lazzarini, P. A., Janda, M., and Reed, L. F., "The validity and reliability of remote diabetic foot ulcer assessment using mobile phone images," *Scientific Reports* **7**, 9480 (Dec. 2017).

[4] Barton, A. A. and Barton, M., "THE CLINICAL AND THERMOGRAPHICAL EVALUATION OF PRESSURE SORES," *Age and Ageing* **2**(1), 55–75 (1973).

[5] Serbu, D. G., "Infrared imaging of the diabetic foot," 8 (2009).

[6] Nakagami, G., Sanada, H., Iizaka, S., Kadono, T., Higashino, T., Koyanagi, H., and Haga, N., "Predicting delayed pressure ulcer healing using thermography: a prospective cohort study," *Journal of Wound Care* **19**, 465–472 (Nov. 2010).

[7] Kanazawa, T., Kitamura, A., Nakagami, G., Goto, T., Miyagaki, T., Hayashi, A., Sasaki, S., Mugita, Y., Iizaka, S., and Sanada, H., "Lower temperature at the wound edge detected by thermography predicts undermining development in pressure ulcers: a pilot study: Lower temperature at the wound edge predicts undermining development in pressure ulcers," *International Wound Journal* **13**, 454–460 (Aug. 2016).

[8] Alametsä, J., Oikarainen, M., Perttunen, J., Viik, J., and Vaalasti, A., "Thermal imaging in skin trauma evaluation: observations by CAT S60 mobile phone," *Finnish Journal of eHealth and eWelfare* **10** (May 2018).

[9] Cwajda-Białasik, J., Mościcka, P., Jawień, A., and Szewczyk, M. T., "Infrared thermography to prognose the venous leg ulcer healing process—preliminary results of a 12-week, prospective observational study," *Wound Repair and Regeneration* , wrr.12781 (Nov. 2019).

[10] Chang, M.-C., Yu, T., Luo, J., Duan, K., Tu, P., Zhao, Y., Nagraj, N., Rajiv, V., Priebe, M., Wood, E. A., and Stachura, M., "Multimodal Sensor System for Pressure Ulcer Wound Assessment and Care," *IEEE Transactions on Industrial Informatics* **14**, 1186–1196 (Mar. 2018).

[11] Mendonça, A. C., Júnior, J. A. F., Frade, M. A. C., Barbosa, R. I., das Neves, L. M. S., de Jesus Guirro, R. R., and de Oliveira Guirro, E. C., "Thermographic Characterization of Cutaneous Ulcers of Different Etiologies," *Journal of Medical Systems* **44**, 160 (Sept. 2020).

[12] Barone, S., Paoli, A., and Razionale, A. V., "Assessment of Chronic Wounds by Three-Dimensional Optical Imaging Based on Integrating Geometrical, Chromatic, and Thermal Data," *Proceedings of the Institution of Mechanical Engineers, Part H: Journal of Engineering in Medicine* **225**, 181–193 (Feb. 2011).

[13] Moghadam, P., "3D medical thermography device," 94851J (May 2015).

[14] Truong, T. P., Yamaguchi, M., Mori, S., Nozick, V., and Saito, H., "Registration of RGB and Thermal Point Clouds Generated by Structure From Motion," in [*2017 IEEE International Conference on Computer Vision Workshops (ICCVW)*], 419–427, IEEE, Venice (Oct. 2017).

[15] AliceVision, "Meshroom: A 3D reconstruction software.," (2018).

[16] Gutierrez, E., Castañeda, B., and Treuillet, S., "Correction of Temperature Estimated from a Low-Cost Handheld Infrared Camera for Clinical Monitoring," in [*Advanced Concepts for Intelligent Vision Systems*], Blanc-Talon, J., Delmas, P., Philips, W., Popescu, D., and Scheunders, P., eds., **12002**, 108–116, Springer International Publishing, Cham (2020). Series Title: Lecture Notes in Computer Science.

[17] Wannous, H., Treuillet, S., and Lucas, Y., "Supervised Tissue Classification from Color Images for a Complete Wound Assessment Tool," in [*2007 29th Annual International Conference of the IEEE Engineering in Medicine and Biology Society*], 6031–6034, IEEE, Lyon, France (Aug. 2007).

[18] Rania, N., Douzi, H., Yves, L., and Sylvie, T., "Semantic Segmentation of Diabetic Foot Ulcer Images: Dealing with Small Dataset in DL Approaches," in [*Image and Signal Processing*], El Moataz, A., Mammass, D., Mansouri, A., and Nouboud, F., eds., 162–169, Springer International Publishing, Cham (2020).